ADVANCED OPTICAL MATERIALS
www.advopticalmat.de

Phonon Analysis of 2D Organic-Halide Perovskites in the Low- and Mid-IR Region

Yan-Fang Chen, Arup Mahata, Aura D. Lubio, Marco Cinquino, Annalisa Coriolano, Lilian Skokan, Young-Gyun Jeong, Luca Razzari, Luisa De Marco, Andreas Ruediger, Filippo De Angelis,* Silvia Colella, and Emanuele Orgiu**

Combining the characteristics of hybrid perovskites and layered materials, 2D Ruddlesden–Popper perovskites exhibit unique properties, some of which still require to be deeply understood. In this study, the vibrational signatures of such materials are analyzed by collecting experimental Raman spectra of four distinct compounds. Supported by density functional theory simulations, the role of the phenyl spacer single fluorination on the phonon modes of two similar yet different compounds, i.e., phenethylammonium lead iodide (PEAI) and 4-fluorophenethylammonium lead iodide (PEAI-F), is explained. In addition, this work analyzes some so-far unreported experimental Raman peaks in the 600–1100 cm^{-1} range and discusses their origin in this class of 2D compounds. This work paves the way for a better design of novel compounds as well as for their exploitation in (opto)electronic applications.

1. Introduction

Hybrid perovskites have garnered significant attention within the scientific community since the revamping of their photovoltaic properties in 2009,[1] and the demonstration of their immense potential.[2] Over a decade afterwards, while vigorous academic and industrial research is still focusing on "archetypical" hybrid 3D perovskites, a vivid interest has emerged for their derivatives with reduced dimensionality.

The general formula of 2D perovskites is A_2BX_4, where A is a monovalent organic cation, B is a divalent metallic cation (for example Pb), and X is a halide anion (Cl, Br, or I). 2D perovskites consist of alternating organic (A) and inorganic layers ($[BX_6]^{4-}$ octahedra), where A acts as an electronically insulating spacer that strongly confine excitons in the inorganic part, forming a natural multiple quantum well.

In particular, layered 2D Ruddlesden–Popper perovskites combine some of the outstanding physical properties of hybrid 3D perovskites with the unique tunability of low-dimensional materials.[3–5] As a result of dielectric confinement, the excitons in 2D perovskites are stable and show strong photoluminescence up to room temperature, unlike the artificially constructed quantum well structures of the classical III–V semiconductors (for example, the GaAs-based heterostructures). For these reasons 2D perovskites have become one of the forefronts

Y.-F. Chen, A. D. Lubio, L. Skokan, Y.-G. Jeong, L. Razzari, A. Ruediger, E. Orgiu
Institut national de la recherche scientifique
Centre Énergie Matériaux Télécommunications
1650 Blv. Lionel-Boulet, Varennes QC J3X 1P7, Canada
E-mail: emanuele.orgiu@inrs.ca

A. Mahata, F. De Angelis
CompuNet
Istituto Italiano di Tecnologia
Via Morego 30, Genova 16163, Italy
E-mail: filippo@thch.unipg.it

A. Mahata, F. De Angelis
Computational Laboratory for Hybrid/Organic Photovoltaics (CLHYO)
Istituto CNR di Scienze e Tecnologie Chimiche "Giulio Natta" (CNR-SCITEC)
Via Elce di Sotto 8, Perugia 06123, Italy

The ORCID identification number(s) for the author(s) of this article can be found under https://doi.org/10.1002/adom.202100439.

DOI: 10.1002/adom.202100439

A. Mahata
Department of Chemistry
Indian Institute of Technology Hyderabad
Kandi, Sangareddy, Telengana 502285, India

M. Cinquino, A. Coriolano, L. De Marco
CNR NANOTEC Institute of Nanotechnology
Via Monteroni, Lecce 73100, Italy
E-mail: luisa.demarco@nanotec.cnr.it

M. Cinquino, A. Coriolano
Dipartimento di Matematica e Fisica E. De Giorgi (Campus Ecotekne)
Università Del Salento
via Monteroni, Lecce 73100, Italy

F. De Angelis
Department of Chemistry, Biology and Biotechnology
University of Perugia
Via Elce di Sotto 8, Perugia 06123, Italy

F. De Angelis
Department of Mechanical Engineering, College of Engineering
Prince Mohammad Bin Fahd University
P.O. Box 1664, Al Khobar 31952, Kingdom of Saudi Arabia

S. Colella
CNR NANOTEC Institute of Nanotechnology
Via Amendola, 122/D, Bari 70126, Italy

of advanced material researches, in particular for their potential for optoelectronic applications.[6–9]

If such materials are to be integrated in optoelectronic devices, studying their vibrational properties is of vital importance as the latter ones can and will also affect the electronic properties through, for example, electron–phonon coupling, thermal expansion of the crystal, or changes in specific heat. Though inelastic neutron scattering is generally considered as the most comprehensive experimental technique to quantitatively explore phonon dynamics over the whole Brillouin zone, it cannot be performed in simple laboratory settings, typically requiring access to large-scale facilities. On the other hand, vibrational spectroscopic techniques such as Raman scattering and THz absorption can provide accurate and reliable characterization of the vibrational modes of many categories of materials. Raman and THz spectroscopies are generally limited to phonons near the Brillouin zone center, except when this restriction is lifted in some specific cases. In particular, this could happen in layered materials where the possible existence of confined modes can allow part of the far-from-center phonons (in the sense of the bulk modes of the materials constituting the individual layers) to be observed through optical methods.[10] On the other hand, the so-called zone-folding effect, where the Brillouin zone of the layered material is considered as "folded" from the zones of the constituting layers, also plays a major role in the interpretation of the observed phonon vibrations.[10] These modes have long been experimentally observed and confirmed in semiconducting superlattices grown by molecular-beam epitaxy.[11–16] Recently, Dahod et al.[17] have proposed using the Rytov model, first used in seismic tomography and then expanded to describe the vibrations in layered materials,[18,19] to account for the low-frequency (<30 cm^{-1}) Raman features of layered hybrid perovskite materials. However, due to the difficulty in obtaining the precise material parameters, the assignment cannot be considered definite.

In our study, four types of 2D hybrid perovskites crystals with various species of organic spacers and identical inorganic framework ($[PbI_6]^{4-}$) are investigated (see structures in **Figure 1**) and studied with Raman spectroscopy, with additional comparison data from THz spectroscopy, to elucidate the influence of the organic ligands on the vibrational modes. In particular, two perovskites having a benzene ring (namely PEAI and PEAI-F, shown in the sketches in Figure 1a) and two perovskites having linear alkyl chains with different lengths (namely BAI and OCT, Figure 1b) have been selected.

With the help of density functional theory (DFT) simulations, insights into the effect of the molecular spacer on the crystal vibrations are obtained. However, some features on the experimental spectra appeared to be inconsistent with the simulation results which, in accord with the general one phonon Raman scattering restrictions, only considered the phonon response near the center of the Brillouin zone. Thus, such a serendipitous inconsistency prompted us to take into account the superlattice effect, extending the work of Dahod et al. into a higher frequency region and suggesting, for the first time, the observation of superlattice confined modes.

2. Results and Discussion

We first focused on the most well-known 2D perovskite among the four derivatives, i.e., phenethylammonium lead iodide (PEAI), composed of a Pb-I inorganic framework and phenethylammonium ions as the organic spacer in between the inorganic layers (Figure 1a, up). Being one of the first demonstrated example of this family of layered structures,[20] various

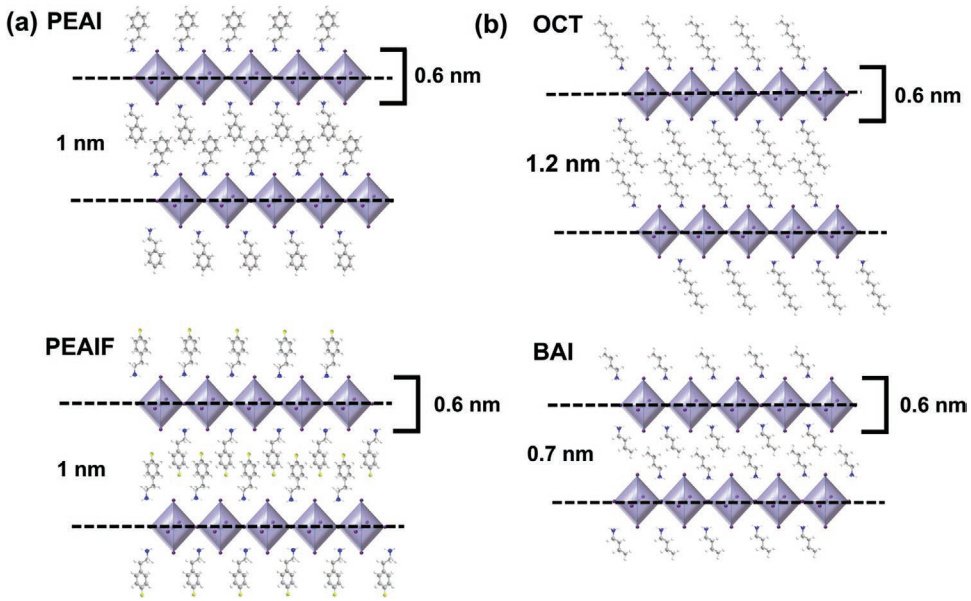

Figure 1. Sketches of the 2D perovskites investigated in this study, their organic ligands, and their approximate structure dimensions: a) Phenethylammonium lead iodide perovskite (PEAI) and 4-fluorophenethylammonium lead iodide perovskite (PEAI-F). In PEAI-F, a fluorine atom replaces a hydrogen atom in *para* position on the benzene ring. b) Octylammonium lead iodide perovskite (OCT) and butylammonium lead iodide perovskite (BAI). The former includes the longer alkyl chain with eight carbon atoms, while in the latter the alkyl chain is of four carbon atoms. This allows to tune the distance between the inorganic layers, causing the interlayer length reducing from 1.2 to 0.7 nm.

experimental and theoretical observations on PEAI were carried on, including exciton properties,[21–23] polaron signature,[24] polariton interactions,[25] and opto-spin effects,[26] while the properties of 2D perovskite with other kinds of spacers have also been under the spotlight.[4,6] Specifically to our study, the vibrational properties of PEAI 2D perovskites have been probed using Raman spectroscopy as previously reported,[27,28] and the assignment of the spectral lines to the simulated vibrational modes to obtain a satisfying description of the measured spectra has been shown to be possible. However, due to the "soft" nature of the hybrid perovskite materials and the formation process via self-assembly,[29] inherently disordered crystals or polycrystalline films at room temperature and above are generally formed,[30] obscuring identifiable Raman peaks. Therefore, most of the Raman studies in hybrid perovskites have to resort to lowering the sample temperature in order to obtain clear enough spectra for the comparison with simulations, sometimes all the way to cryogenic temperatures.[27,28,31] On the other hand, a study at room temperature is of utter importance, as it is at this temperature that most device applications are conceivable. Further, the vibrational properties of the 2D perovskites are expected to change drastically at low temperature, due to the occurrence of crystalline phase transition at temperatures as high as 250 K.[32,33] We found that this dilemma (no clear spectra can be obtained at temperatures where the interest lies) can be resolved by the optimized selection of the excitation wavelength in the Raman measurement: by choosing a wavelength that is as short as possible to increase the Raman activity to obtain higher signal-to-noise ratio, but not so short that it introduces photoluminescence in the sample. In the case of 2D perovskites, whose optical bandgap is ≈2.5 eV (see Figure S2, Supporting Information), a helium-neon laser (633 nm, corresponding to a photon energy of 1.96 eV) meets the requirements. Such measurement conditions, combined with high quality single crystalline samples (for preparation details, see the Experimental Section), provide the opportunity of resolving the spectral features at room temperature.

The measured Raman spectrum of PEAI is shown in **Figure 2**b (dark green line). Surprisingly, strikingly different features, compared to the spectra obtained using lower photon energies,[17,27,28] can be observed. Generally, a few groups of peaks are observed in this frequency range while, in Figure 2b, several peaks with width of tens of cm^{-1} overlapping on an increasing background toward low wavenumbers could be observed. Following the assignments widely accepted within the (hybrid perovskite) literature,[34–37] and, more specifically Yaffe et al.,[30] we identify the origin of the broad peaks to be the phonon vibrations in the crystal, while the background is an example of Raman central peaks,[38–40] resulting from the continuous polar fluctuations occurring in the material.

Further understanding of the origin of the features can be obtained by comparison with the complementary THz spectra (Figure 2c, dark red line). Note that the signal-to-noise ratio of

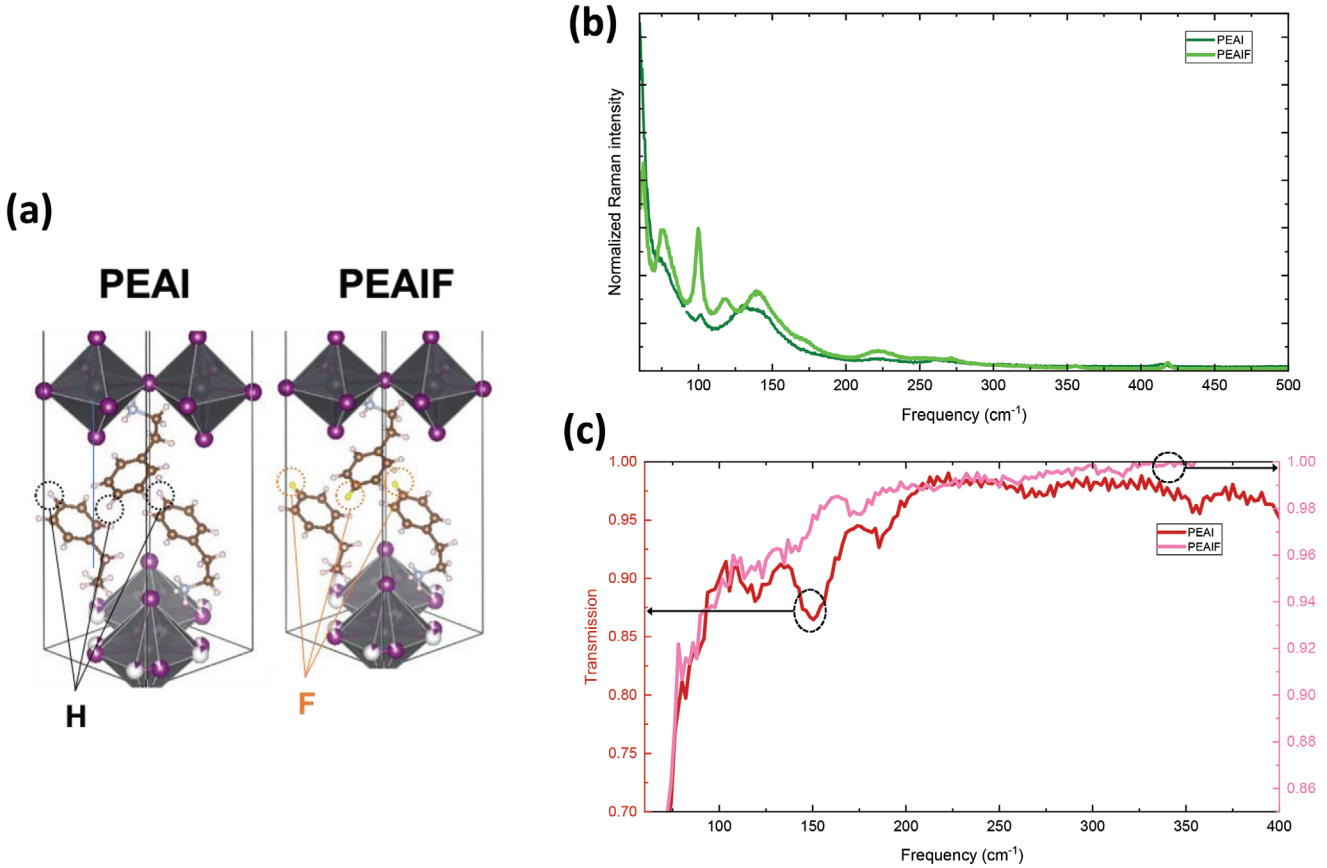

Figure 2. Experimental low-wavenumber vibrational spectra of phenethylammonium lead iodide perovskite (PEAI) and 4-fluorophenethylammonium (PEAI-F) 2D perovskites: a) Schematics of the crystal structures of the two perovskites. b) Raman spectra (λ_{ex} = 633 nm). c) THz spectra of thin crystals.

this set of spectra suffered greatly from the partial and uneven sample coverage (see Figure S1, Supporting Information), mainly owing to the size of the illuminated region in the THz measurements (of the order of a few square millimeters) compared to the few μm^2 of the focused laser spot used in Raman spectroscopy. However, a few resonant features with width of a few tens of cm^{-1} (similar to those in the Raman spectra) could still be identified. The positions of the observed features in the two spectra do not correspond, confirming the phonon assignment as it is widely expected that the selection rules for the Raman process and infrared process (THz absorption) are different, resulting in different groups of optical phonons being activated.

As discussed in the introduction, we then carried out the same spectroscopic characterization on PEAI-F 2D perovskite to better understand the intriguing observed features. PEAI and PEAI-F only differ by the presence of a fluorine atom in place of a hydrogen in *para* position on the benzene ring (see sketches in Figure 2a)[41], as determined by X-ray diffraction measurements reported in previously published papers.[42–44] The fluorination of 2D perovskites allowed to compare straightforwardly the two sets of spectra and to analyze in detail the role of the hydrogen/fluorine atom in the organic spacer, as exampled by the temperature dependent photoluminescence spectroscopy study by Tekelenburg et al.[45]

The Raman and THz spectra of the PEAI-F samples are shown in Figure 2b,c (lighter lines), respectively. Similar spectral features to that of PEAI are observed, with minor frequency shift and, in some cases, what appears to be a peak splitting. A general consideration on the structural compositions helps to gain some insight into the observed difference: The fluorine substitution results in a "stiffer" crystal, resulting in higher phonon frequencies (see, for instance, the peaks around 75, 100, and 225 cm^{-1} in Figure 2b). Indeed, as shown by Tu et al.,[46] the organic spacer has notable effects on the elastic properties of the 2D perovskites, and it is likely that the introduction of fluorine increases the bond strength and therefore the rigidity of the spacer. The splitting of the PEAI peak centered around 125 cm^{-1} into two peaks in the case of PEAI-F can be linked to the lifting of the degeneracy in this particular branch of phonons as a result of the substitution.

Moving beyond the qualitative descriptions above, we carried out density functional perturbation theory (DFPT). Following the general density functional theory framework but perturbating the positions of individual atoms to calculate the force matrices, DFPT can be used to simulate the phonon dispersion relations and the resulting phonon density-of-state, or, by additionally calculating the second and third derivative of the permittivity, the Raman and infrared activity of the material.[47,48] We note that DFPT simulations capture mostly the static part of the spectroscopic response, and, as such they are unable to describe the dynamics of the system. Such a shortcoming can be overcome to a certain extent by the inclusion of molecular dynamics simulation.[30] Another aspect that can modify the phonon structure of hybrid perovskite materials is the anharmonic effects,[49–51] whose experimental probing generally involves temperature dependent measurements.[52]

As described more in detail within the Experimental Section, the DFPT simulated Raman and infrared activity of the PEAI and PEAI-F 2D perovskites are shown in **Figure 3**a,b, respectively. As can be observed from Figure 3, even with the finite temperature broadening effect taken into account and considering the simplifying conditions used in the simulations, the overall qualitative similarity between the simulated and experimental spectra seems to be lacking. For example, in the experimental spectra, one of the most notable features is the rapid decrease of Raman intensity with increasing wavenumber observed in the experimental spectra, but this can hardly be conceived to be reproduced by the simulation. Such discrepancy between DFPT simulation and experiment is not rare in the literature, in different kinds of materials or even hybrid perovskites,[5,36] but is rarely directly addressed, as multiple influencing factors might be at play, both computationally and experimentally. However, in this case we note that the layered nature of our samples presents some unique possibilities of lifting the Raman and infrared selection rules, as mentioned earlier, and therefore the experimental spectra could also likely include phonons from all over the Brillouin zone. In such cases, the phonon density of states (pDOS) will provide valuable information concerning the nature of the observed vibrational states.

The simulated pDOS of PEAI and PEAI-F 2D perovskites are shown in Figure 3c. The main difference in the simulated pDOS between PEAI and PEAI-F arises in the frequency range between ≈75–200 cm^{-1}, which is approximately in the same region where the experimental spectra show the most differences. A closer examination of the simulation results, including the visualization of the individual vibrational modes, shows that PEAI-F presents additional modes in this frequency region. Specifically, the 4-fluorophenethylammonium ion flipping along with Pb-I stretching modes at 78.52 and 84.85 cm^{-1} and the 4-fluorophenethylammonium ion flipping modes at 131.13 and 157.05 cm^{-1} do not have corresponding peaks on the of PEAI spectra (Figure 3c, the indicated mode positions and the vector diagrams). These additional modes are a result of the much heavier fluorine atom restricting the phenyl ring rotations within its equatorial plane and promoting the axial flipping motions with respect to the 1-to-4 diagonal carbon atoms of the phenyl ring. The vector diagrams of the fluorine induced modes are shown in Figure 3c. Additional analysis of the pDOS simulation compared with $MAPbI_3$ is also of great interest as it provides another examination of how the organic molecules affect the vibrational motion and can be found in the supporting information.

In order to better understand the role played by the phenyl rings on the Raman activity in this frequency region, we next turn our attention to two other kinds of 2D perovskites whose organic spacer is either an 8-carbon (OCT) or a 4-carbon (BAI) alkyl chain (see **Figure 4**a). The Raman spectra, obtained upon excitation at a photon energy close to the bandgap width, are shown in Figure 4b. The features of OCT and BAI were found to be similar to those of PEAI and PEAI-F: broad phonon peaks overlapped with central peaks resulting from polar fluctuations were observed. It seems like that the overall features of the BAI spectrum are shifted toward higher frequencies than those of OCT, which again can be intuitively explained as the result of a "stiffer" crystal structure resulting from shorter alkyl chains.

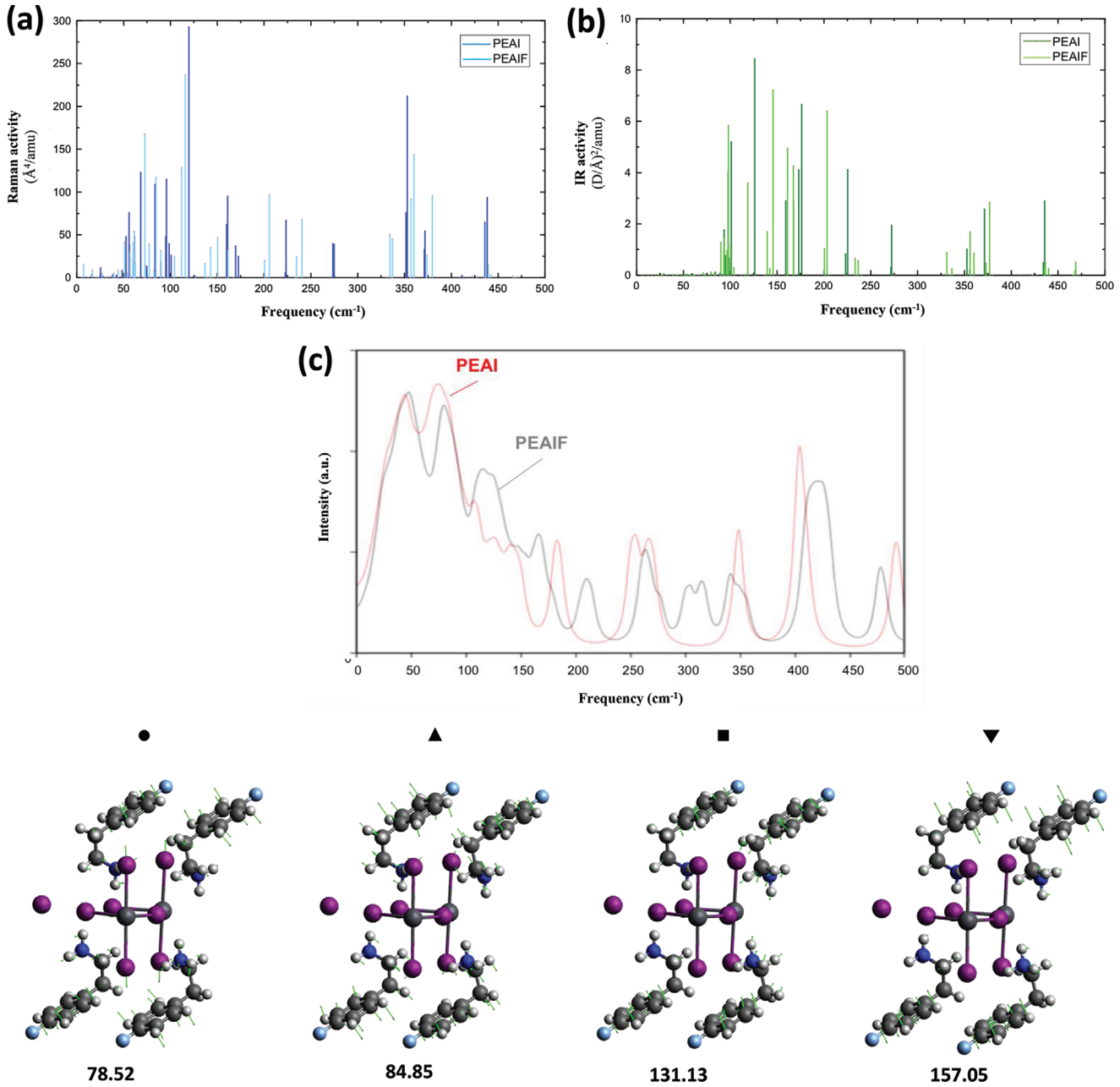

Figure 3. Density functional perturbation theory (DFPT) simulation of the vibrational modes in phenethylammonium lead iodide (PEAI) and 4-fluorophenethylammonium lead iodide (PEAI-F) perovskites: a) Raman active modes with their activity in ang^4amu^{-1}. b) IR active modes with their intensity in $D^2ang^2amu^{-1}$. c) Total phonon density of states. Additional modes in PEAI-F are visualized in the bottom graphs. The green arrows attached to the atoms indicate the vibrational amplitudes of each mode. As the arrows are presented mostly on the phenyl rings of the 4-fluorophenethylammonium ion, these modes are associated with the ion flipping modes, as discussed in the text.

The Raman and infrared activity of OCT and BAI simulated using DFPT are shown in **Figure 5**a,b, respectively. As with the case of PEAI and PEAI-F, the similarity between simulation and experiment seems to be lacking, further confirming our suggestion that, in these layered materials, the k-vector preservation has been modified, and therefore the total pDOS should be taken into account (Figure 5c). A closer examination into the frequency region where the spacers play an important rule (75–200 cm^{-1}) shows that this region is dominated by the motions of the alkyl chains: For BAI, the libration motions along the C2-C3 bonds appear at 130, 131, 133, and 134 cm^{-1}, while at 128, 131, 138, and 140 cm^{-1} in the case of OCT. The librations of the NH_3 groups occurs at 176, 179, 186, and 189 cm^{-1} for BAI, and 176, 179, 180, and 182 cm^{-1} for OCT. Additional peaks emerging from the longer chains of OCT are at 142, 142, 144, and 145 cm^{-1} and at 156, 161, 164, and 166 cm^{-1}.

Though these peaks are difficult to distinguish on the experimental spectra, we note that in this region no marked peaks

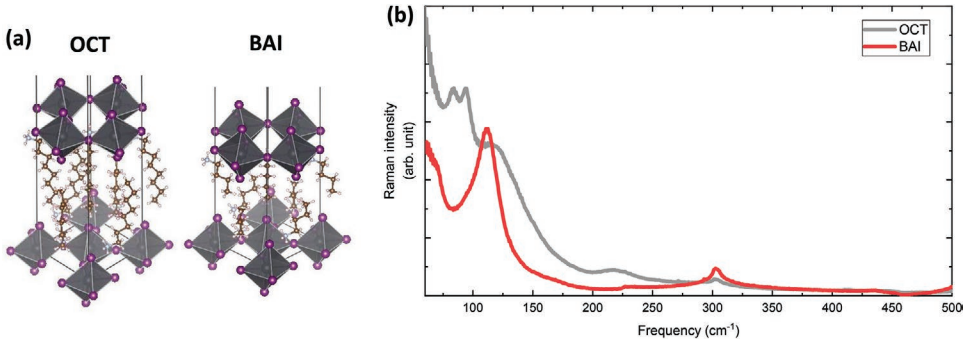

Figure 4. a) Crystalline structure of octylammonium lead iodide perovskite (OCT) and butylammonium lead iodide perovskite (BAI). b) Experimental Raman spectra (at low wavenumber) of OCT and BAI 2D perovskites (λ_{ex} = 633 nm). The peaks around 230 and 300 cm^{-1} originate from the silicon substrate (see Figure S7, Supporting Information).

were observable experimentally, consistent with the simulation in that multiple modes are contributing and hence their broadening "blurs out" the overall spectra. Additionally, unlike the case of PEAI versus PEAI-F, the Raman spectra of OCT versus BAI seem to display a higher resemblance in that the peak splitting is not observable in the latter case, which serves as an indication of the similarity of the active modes in this region. This is consistent with the idea that the additional modes introduced by the longer alkyl chain do not lead to substantial structural changes, which are most likely responsible for the observed peak splitting, as a result of the fluorine substitution (that introduces additional flipping motion of the organic spacers). A more detailed analysis of the 200–300 cm^{-1} region can be found in the Supporting Information.

After examining the role played by the organic spacers on the vibrational properties in the low wavenumber range (i.e., 70–500 cm^{-1}), we note that among the Raman spectra of the four kinds of 2D perovskites, a striking pattern seems to repeat itself: certain notable peaks pair with each other with a frequency splitting of the order of 10 cm^{-1} (see Figure 2b, around 80, 125, and 230 cm^{-1}; Figure 4b, around 110 cm^{-1}). An earlier study suggested that the existence of such pairwise peaks could be a signature of the zone-folded modes that is the result of a folded Brillouin zone occurring in superlattices.[10] As discussed in the introduction, the existence of such modes in 2D perovskites has been proposed by Dahod et al.,[17] although in a much lower frequency region (≈<30 cm^{-1}). We note that, therefore, it is not completely unreasonable to investigate the possibility

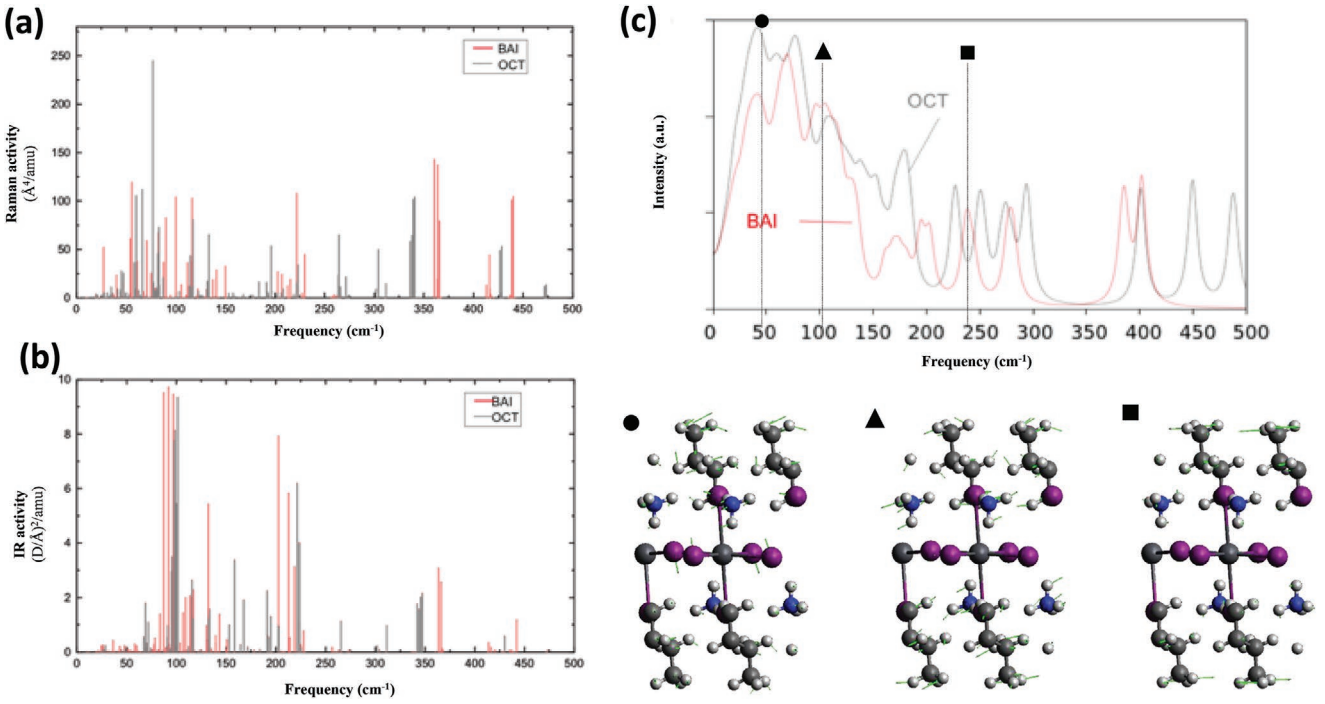

Figure 5. Density functional perturbation theory (DFPT) simulation of the vibrational modes in butylammonium lead iodide perovskite (BAI) and octylammonium lead iodide perovskite (OCT) perovskites: a) Raman active modes. b) IR active modes. c) Total phonon density with representative modes. As above, the green arrows indicate the vibrational amplitudes of the modes, showcasing the motions of the atoms.

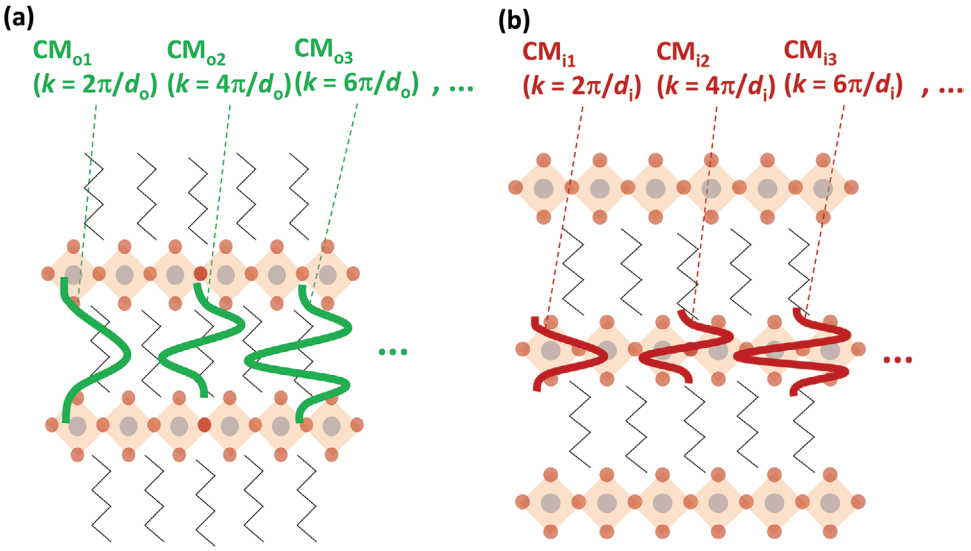

Figure 6. Confined-mode solution of the alternating linear chain model: a) Modes confined within an organic layer and b) confined within an inorganic layer.

that these pairwise peaks as the higher order zone-folded superlattice modes originating from the sub-30 cm^{-1} region.

Besides the zone-folded modes, other widely studied superlattice modes are the so-called localized modes or confined modes, in which the vibrations are mostly confined within one of the layers of the superlattice (**Figure 6**). To satisfy the nullifying boundary condition, the wavenumbers of such modes are quantized into:

$$n\frac{2\pi}{d} \tag{1}$$

where d is the thickness of the layer in which the phonon is confined, and n is a natural number.[10,53,54] The confined-mode phonon Raman response has been established in GaAs/AlAs superlattices and in other previous studies.[11–14] For 2D perovskites, though the structural similarity to superlattice is only apparent, no such assignment has been suggested in the literature so far, to the best of our knowledge. Besides the relative structural complexity of 2D perovskites, the major difficulty of such assignment lies in the ill-defined material parameters: the packing of the PbX_6^{-4} framework and organic spacers are nowhere near their free-standing structures, resulting in vastly different elastic and dielectric constants, making modeling from these parameters very difficult to obtain, contrary to the case of GaAs/AlAs superlattices,[55] where the individual layers are well-defined.

Qualitatively, though, one might expect that the modes trapped in the inorganic framework (Figure 6b) would be largely indifferent to the composition of the organic spacers, as long as the interaction between the layers does not significantly affect the orientation of the PbX_6^{-4} octahedra. This is the case for the four kinds of samples used in this study, where the Pb-I-Pb angles range from 152° to 156°.[42,56–58] Therefore, the identification of these "invariant" modes between different spacer compositions could, in first approximation, provide an indication of the confined modes.

One such set of modes appears in the frequency region of 600 to 1100 cm^{-1} (**Figure 7**). First, we note that, compared with

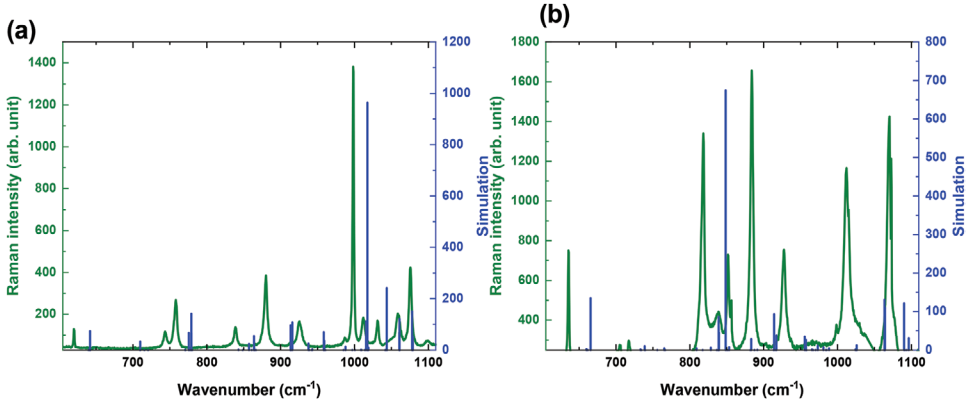

Figure 7. Experimental Raman modes in the 600 to 1100 cm^{-1}frequency range for a) phenethylammonium lead iodide (PEAI) and b) 4-fluorophenethylammonium lead iodide (PEAI-F) 2D perovskites. (Green lines: measured Raman intensity. Blue lines: density functional perturbation theory (DFPT) simulated Raman activities.)

Table 1. Observed mode frequencies in the range of 600 to 1100 cm^{-1}. The commonly observed modes are highlighted in bold.

	PEAI	PEAI-F	Average position of the common peaks	Difference between subsequent peak positions
Mode frequencies [cm^{-1}]	**1076**	**1070**	1073	61
	1058	**1012**	1012	85
	1031	**928**	927	88
	1012	884*	839	92
	998*	852	747	
	987	818*		
	926	**839**		
	914	**750**		
	880*	717		
	839	635*		
	800			
	758*			
	744			
	700			
	620*			

DFPT simulation of Raman activity, multiple unaccounted-for peaks appear in this frequency region, most strikingly in the case of PEAI-F (Figure 7b). The appearance of these modes gives the first evidence that different mechanisms might be at play, as generally the DFPT simulation in hybrid perovskite materials gives more than enough modes for experimental spectra to identify with due to the large number of atoms in the unit cells and the lack of directional symmetries.

The observed mode frequencies in this region are listed in **Table 1**, in which one can clearly observe a subset of almost identical peak positions (difference less than 1%, bold in Table 1). Interestingly, the spacing between the subsequent common peaks (Table 1, last column) shows a steady increase toward lower frequencies. Taking into account the fact that the ω-versus-k phonon dispersion relations are generally slightly concave, this behavior is consistent with the quantized confined phonon wavenumbers: As the confined phonons are equally separated in the k-space (Equation (1)), the differences between mode positions should be increasing when assigning the highest-frequency peak to be $n = 1$, second highest peak to be $n = 2$, etc.

The existence of the unaccounted-for peaks commonly observed between different organic spacers with their frequency spacing increasing toward lower frequencies thus provides the basis to tentatively assign these modes to the superlattice confined modes in the inorganic framework (CM_i in Figure 6b). Following this reasoning, it is possible that the remaining peaks in Table 1 may arise from confined modes in the organic layer (CM_o in Figure 6a) if their spacing follows the same trend (increases toward lower frequencies), and, indeed, such subsets can be found in both compositions, as indicated by the asterisks in Table 1. These two subsets (CM_i and CM_o) thus account for over two-thirds of the peaks in this frequency region. The remaining peaks, in similar compounds, were suggested to originate from molecular vibrations within the organic layers,[59,60] or further superlattice modes.[61,62]

Returning to the spectra and assigning the CM_i and CM_o modes to the peaks as discussed (**Figure 8**), it can be observed that the peak intensities decrease monotonically with mode index n (see Equation (1)), in agreement with the trend observed in GaAs/AlAs superlattices,[11–14] and generally expected in higher order modes. Assuming the layer thickness of the inorganic framework to be about two-third of the total thickness, constructing the simplified linear chain model,[10] we can then plot the dispersion relation of the two branches of the confined phonons in PEAI and PEAI-F (**Figure 9**). As discussed before, the inorganic branches of PEAI and PEAI-F overlap with each other, while the organic branches intercept with the inorganic branches.

In terms of the absolute frequencies of these branches though, we note that there is a possibility that what we are observing in this frequency range might be the result of the higher-order Raman scattering that involves multiple confined phonons at once,[63–65] and the single phonon response might not be clearly observable, being blended into the response of other nonlocalized modes. Further clarification on these points constitutes the object of an ongoing work.

Another indication of the nature of the possibly confined modes could perhaps be suggested by the (unexpected) absence in OCT and BAI samples (Figure S6, Supporting Information): No identifiable peaks appear in this frequency range, contrary to the prediction of DFPT simulation. However, the confined mode response has been known to be sensitive to the excitation wavelength,[11,64] or, more specifically, it is subject to specific conditions that involve the ratio between excitation energy and energy gap of the material.[64] Regarding the four materials encompassed in our study, we note that the bandgap of both OCT and BAI is larger than that of PEAI and PEAI-F (Figure S2, Supporting Information). As the excitation wavelength ($\lambda_{ex} = 633$ nm) was fixed in all measurements, the laser energy might not be enough to excite the confined modes of OCT and BAI due to their larger bandgaps.[65]

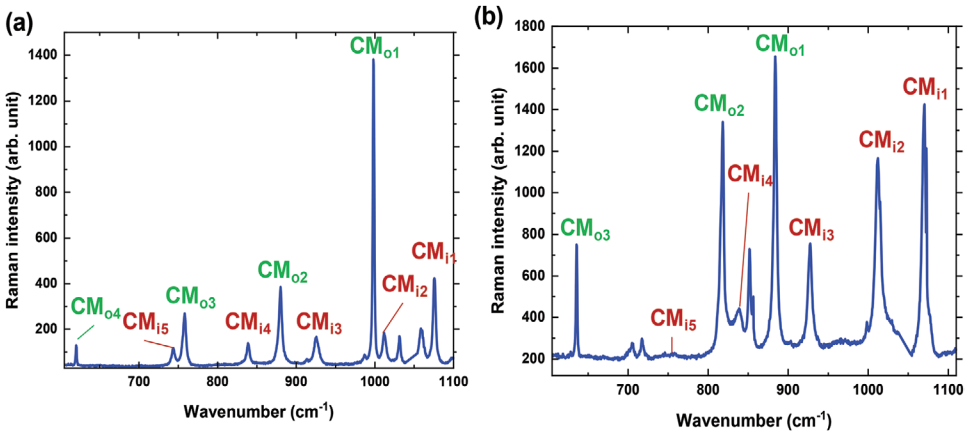

Figure 8. Tentative assignment of the observed peaks to confined modes in a) phenethylammonium lead iodide (PEAI) and b) 4-fluorophenethylammonium lead iodide (PEAI-F) 2D perovskites.

However, in order to prove the very nature of such modes further Raman measurements were carried out on PEAI perovskites with a higher number of octahedral layers, i.e., $n = 2$ and 3 (see Figures S10–S12, Supporting Information). In the case of $n = 2$ and 3, the values of CM_i observed in PEAI with $n = 1$ should not shift while the CM_o values should peak at wavenumbers that are 1/2 or 1/3 of those measured by Raman in PEAI with $n = 1$. The experimental results did not confirm the last assumption. Hence, we emphasize that the assignment of such peaks is not conclusive and more work will be needed in the near future to single out their origin. DFT did not provide any strong candidates for assignment, but further work is required to fully understand these experimental findings.

3. Conclusion

In conclusion, in this study we recorded, analyzed, and simulated the phonon response of four different kinds of layered perovskites. In particular, the role of the single fluorination of the phenyl spacer on the phonon modes of two widely employed 2D perovskite compounds, i.e., PEAI and PEAI-F, was analyzed and found to profoundly affect their Raman spectra. Noteworthy, we measured experimental Raman peaks in the 600–1100 cm^{-1} range and discussed their origin. In spite of the fact that the assignment of such peaks still deserves more computational and experimental efforts to be fully understood, interpretation of the vibrational modes in this class of materials clearly paves the way for a better chemical design as well as for their exploitation in (opto)electronic applications.

Although this work puts forward the analysis of vibrational modes in 2D layered perovskites, it is worth stressing that the understanding of phonons in this novel class of materials is key for an in-depth comprehension of other major physical mechanisms, such as exciton separation in solar cells as well as charge, exciton, and heat transport, all involving interactions between charged or excitonic species and phonons.

4. Experimental Section

Synthesis of 2D Perovskite Single Crystals: PEAI, PEAI-F, BAI, and OCT solutions (0.5 M) were prepared in a nitrogen-filled glovebox by dissolving PbI_2 and phenethylammonium iodide, 4-fluorophenethylammonium iodide, butylammonium iodide, and octylammonium iodide, respectively, (1:2 molar ratio) in γ-butyrolactone and stirring at 70 °C for 1 h.

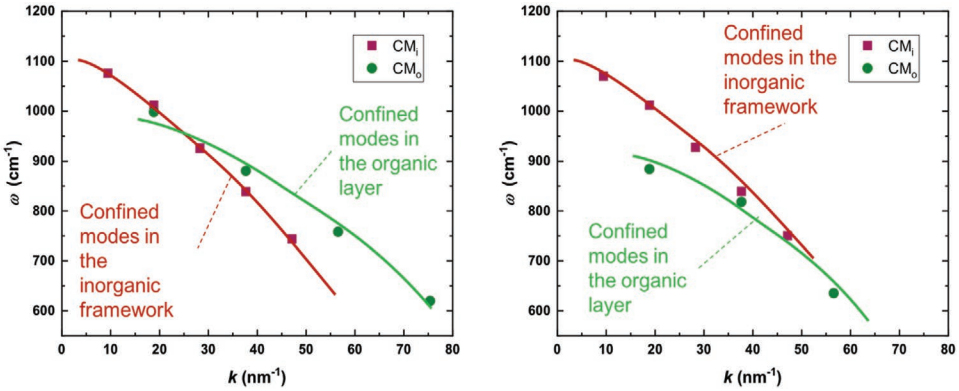

Figure 9. Summary of the experimental results attempting to model confined modes in 2D perovskites. The simplified model of alternating organic "o" and inorganic "i" layers. Dispersion relation of the confined modes of (left) phenethylammonium lead iodide (PEAI) and (right) 4-fluorophenethylammonium lead iodide (PEAI-F) 2D perovskites. The solid lines are guides for the eye.

2D perovskite single crystals are synthesized using an anti-solvent vapor-assisted crystallization method as follows:[25,43,44] 3 µL of perovskite solution are deposited on glass or Si/SiO_2 and covered with glass or Si/SiO_2. Substrates and a small vial containing 2 mL of dichloromethane were placed inside a bigger Teflon vial which is closed with a screw cap and left undisturbed for 12 h at room temperature (see Figure S1a, Supporting Information). As the antisolvent (dichloromethane) saturates the environment and slowly infiltrates the precursor solution, supersaturation is reached and perovskite single crystals begin to form in the gap between the two substrates. At the end of the process, high-quality, millimeter-sized yellow flakes with a thickness of a few microns are obtained (see Figure S1b, Supporting Information). Their thickness varies from few to tens of micrometers. Using SPV 224PR-M Nitto Tape or polydimethylsiloxane (PDMS), mechanical exfoliation is carried out on the perovskite flakes in order to obtain single crystals having the desired thickness (see Figure S1c, Supporting Information).

PEAI perovskite single crystals with a higher number of octahedral layers, i.e., $n = 2$ and 3 were prepared as follows: lead iodide 447 mg, phenethylammonium iodide 46 mg, methylammonium iodide 370 mg, and potassium iodide (1400 mg for $n = 2$, 1000 mg for $n = 3$) were dissolved at 70 °C in a mix of water/acetonitrile (1.05/0.45 mL, respectively). All the precursors were stirred at 70 °C for 1 h producing a bright yellow solution. Then the temperature was raised to 83 °C. After some minutes the crystallization occurs at the water–air interface followed by a fast lateral growth within the water–air plane. Then, crystals were extracted using a net and gently collected and dried with paper in order to remove the remaining perovskite solution.[66]

Raman Spectroscopy: Raman spectroscopy was performed using a linearly polarized helium–neon laser (Melles-Griot 25-LHP-928-249, λ_{ex} = 633 nm, TEM 00, linewidth 12 MHz) with a power of 10 mW in front of the entrance pupil of the confocal objective. The laser beam was focused using a 100× objective with NA = 0.7, resulting a light spot area at the order of 1 µm^2. The backscattering light was collected confocally in a Tokyo Instruments spectrometer with a focal length of 500 mm via a grating of 1800 lines per millimeter with data acquisition time of 5 min to obtain a spectral resolution of approximately 1 cm^{-1}. A thermoelectrically cooled CCD (Andor iDUS 420 BUV) operating at –70 °C was used for detection with reduced dark noise.

Raman spectroscopy on PEAI with $n = 2$ and 3 was performed using a depolarized incident beam (λ_{ex} = 785 nm) with a laser power of 10 mW in front of the entrance pupil of the confocal objective. The estimated spot size was of 3.1 μm (10× objective) while the spectral range spans from 8 to 1846 cm^{-1}. Each sample has 5 spectra taken on different spots of the sample.

THz Spectroscopy: THz spectroscopy is carried out using a dedicated Fourier-transform spectrometer (Blue Sky Spectroscopy Inc.) equipped with a silicon nitride blackbody light source and a pyroelectric detector (QMC Instruments Ltd.). The transmission spectra are retrieved by Fourier transforming the average of 500 interferogram scans with a resulting resolution of 2 cm^{-1}.

pDOS Simulation: The first-principles calculations based on DFT were carried out as implemented in the PWSCF Quantum-Espresso package.[66] Geometry optimization was performed using GGA-PBE level of theory,[67] and the electrons-ions interactions were described by ultrasoft pseudo-potentials with electrons from I 5s, 5p; N, C, F 2s, 2p; H 1s; Pb 6s, 6p, 5d; shells explicitly included in calculations. The experimental cell parameters have been used in all the cases. Geometry optimizations for $2 \times 2 \times 1$ supercell were performed with a k-point sampling of $4 \times 4 \times 2$,[68] along with plane-wave basis set cutoffs for the smooth part of the wave functions and augmented electronic density expansions of 25 and 200 Ry, respectively.

Frequency calculations had been performed by DFPT and by using PBE functional and ultrasoft pseudopotentials with a cutoff on the wavefunction of 25 Ry (200 Ry on the charge density) and uniform $4 \times 4 \times 2$ grid of k-points in the Brillouin zone. Phonon DOS had been plotted from the interatomic force constant in real space, which was calculated from the dynamical matrices produced at Gamma point followed by their Fourier transformation.

Raman and Infrared Activity Simulation: Similarly to the pDOS simulation, the Raman and infrared simulation were carried out with the help of PWSCF Quantum-Espresso package. Due to the intrinsic limitation of the Raman simulation algorithm, the geometry optimization and the subsequent vibrational mode simulation were implemented at the LDA level of theory, with Perdew–Zunger exchange correlation functional, with a cutoff on the wavefunction of 80 and 800 Ry on the charge density and $4 \times 4 \times 2$ grid of k-points in the Brillouin zone.

Supporting Information

Supporting Information is available from the Wiley Online Library or from the author.

Acknowledgements

E.O., A.R., and L.R. were supported by the Natural Sciences and Engineering Research Council of Canada (NSERC) through individual Discovery Grants. A.R. would also like to acknowledge funding from the NSERC Strategic Grant program. E.O. and Y.-F.C. were also supported by the Fonds de Recherche du Québec – Nature et Technologies (FRQNT). A.L. and L.S. wish to thank the FRQNT for their PhD/MSc scholarship. A.R. is grateful to the FRQNT for funding pieces of this research through an Équipe grant. The authors wish to thank Prof. Cyril Muehlethaler (Université du Québec à Trois-Rivières) for granting access to the micro-Raman facilities at his institution. A.M. and F.D.A. acknowledge support from the European Union's Horizon 2020 research and innovation programme under Grant Agreement No. 764047 of the Espresso project. F. D. A. thanks Ministero Istruzione dell'Universita' e della Ricerca (MIUR) and the University of Perugia through the program "Dipartimenti di Eccellenza 2018–2022" (grant AMIS). L.D.M., A.C., and M.C. gratefully acknowledge Apulia Region, project "Progetto Tecnopolo per la Medicina di precisione", grant number: Deliberazione della Giunta Regionale n. 2117 del 21/11/2018 and Ministry of University and Scientific Research (MIUR), project FISR—C.N.R. "Tecnopolo di nanotecnologia e fotonica per la medicina di precisione", grant number: CUP B83B17000010001 for funding.

Open Access Funding provided by Consiglio Nazionale delle Ricerche within the CRUI-CARE Agreement.

Conflict of Interest

The authors declare no conflict of interest.

Data Availability Statement

The data that support the findings of this study are available from the corresponding author upon reasonable request.

Keywords

2D perovskites, DFT simulations, phonons, Raman spectroscopy

Received: March 1, 2021
Revised: March 13, 2022
Published online: June 16, 2022

[1] A. Kojima, K. Teshima, Y. Shirai, T. Miyasaka, *J. Am. Chem. Soc.* **2009**, *131*, 6050.
[2] M. M. Lee, J. Teuscher, T. Miyasaka, T. N. Murakami, H. J. Snaith, *Science* **2012**, *338*, 643.
[3] K. Zheng, T. Pullerits, *J. Phys. Chem. Lett.* **2019**, *10*, 5881.
[4] L. Mao, C. C. Stoumpos, M. G. Kanatzidis, *J. Am. Chem. Soc.* **2019**, *141*, 1171.
[5] C. M. Mauck, W. A. Tisdale, *Trends Chem.* **2019**, *1*, 380.
[6] F. Zhang, H. Lu, J. Tong, J. J. Berry, M. C. Beard, K. Zhu, *Energy Environ. Sci.* **2020**, *13*, 1154.
[7] J. Wong, K. Yang, *Sol. RRL* **2021**, *5*, 2000395.
[8] I. C. Smith, E. T. Hoke, D. Solis-Ibarra, M. D. McGehee, H. I. Karunadasa, *Angew. Chem., Int. Ed. Engl.* **2014**, *53*, 11232.
[9] T. Luo, Y. Zhang, Z. Xu, T. Niu, J. Wen, J. Lu, S. Jin, S. Liu, K. Zhao, *Adv. Mater.* **2019**, *31*, 1903848.
[10] B. Jusserand, M. Cardona, in *Light Scattering in Solids V: Superlattices and Other Microstructures* (Eds: M. Cardona, G. Guntherodt), Springer-Verlag Berlin Heidelberg, Germany **1989**, Ch. 3.
[11] A. K. Sood, J. Menéndez, M. Cardona, K. Ploog, *Phys. Rev. Lett.* **1985**, *54*, 2111.
[12] Z. P. Wang, H. X. Han, G. H. Li, D. S. Jiang, K. Ploog, *Phys. Rev. B* **1988**, *38*, 8483.
[13] J. Menéndez, A. Pinczuk, J. P. Valladares, *Appl. Phys. Lett.* **1987**, *50*, 1101.
[14] T. A. Gant, M. Delaney, M. V. Klein, R. Houdré, H. Morkoç, *Phys. Rev. B* **1989**, *39*, 1696.
[15] A. Ishibashi, M. Itabashi, Y. Mori, K. Kaneko, S. Kawado, N. Watanabe, *Phys. Rev. B* **1986**, *33*, 2887.
[16] H. Liu, Y. Zhang, E. H. Steenbergen, S. Liu, Z. Lin, Y.-H. Zhang, J. Kim, M.i-H. Ji, T. Detchprohm, R. D. Dupuis, J. K. Kim, S. D. Hawkins, . F. Klem, *Phys. Rev. Appl.* **2017**, *8*, 034028.
[17] N. S. Dahod, A. France-Lanord, W. Paritmongko, J. C. Grossman, W. A. Tisdale, *J. Chem. Phys.* **2020**, *153*, 044710.
[18] S. M. Rytov, *Sov. Phys. Acoust.* **1956**, *2*, 68.
[19] C. Colvard, R. Merlin, M. V. Klein, A. C. Gossard, *Phys. Rev. Lett.* **1980**, *45*, 298.
[20] J. Calabrese, N. L. Jones, R. L. Harlow, N. Herron, D. L. Thorn, Y. Wang, *J. Am. Chem. Soc.* **1991**, *113*, 2328.
[21] D. B. Straus, C. R. Kagan, *J. Phys. Chem. C* **2018**, *9*, 1434.
[22] J. M. Urban, J. M. Urban, G. Chehade, M. Dyksik, M. Menahem, A. Surrente, G. Trippé-Allard, D. K. Maude, D. Garrot, O. Yaffe, E. Deleporte, P. Plochocka, M. Baranowski, *J. Phys. Chem. Lett.* **2020**, *11*, 5830.
[23] J. Zhang, X. Zhu, M. Wang, B. Hu, *Nat. Commun.* **2020**, *11*, 2618.
[24] S. Neutzner, F. Thouin, D. Cortecchia, A. Petrozza, C. Silva, A. R. S. Kandada, *Phys. Rev. Mater.* **2018**, *2*, 064605.
[25] A. Fieramosca, L. Polimeno, V. Ardizzone, L. De Marco1, M. Pugliese, V. Maiorano, M. De Giorgi, L. Dominici, G. Gigli, D. Gerace, D. Ballarini, D. Sanvitto, *Sci. Adv.* **2019**, *5*, eaav9967.
[26] D. Giovanni, W. K. Chong, H. A. Dewi, K. Thirumal, I. Neogi, R. Ramesh, S. Mhaisalkar, N. Mathews, T. C. Sum, *Sci. Adv.* **2016**, *2*, e1600477.
[27] F. Thouin, S. Neutzner, D. Cortecchia, V. A. Dragomir, C. Soci, T. Salim, Y. M. Lam, R. Leonelli, A. Petrozza, A. R. S. Kandada, C. Silva, *Phys. Rev. Mater.* **2018**, *2*, 034001.
[28] C. M. Mauck, A. France-Lanord, A. C. H. Oendra, N. S. Dahod, J. C. Grossman, W. A. Tisdale, *J. Phys. Chem. C* **2019**, *123*, 27904.
[29] A.C. Ferreira, A. Létoublon, S. Paofai, S. Raymond, C. Ecolivet, B. Rufflé, S. Cordier, C. Katan, M.I. Saidaminov, A.A. Zhumekenov, O.M. Bakr, J. Even, P. Bourges, *Phys. Rev. Lett.* **2018**, *121*, 085502.
[30] O. Yaffe, Y. Guo, L. Z. Tan, D. A. Egger, T. Hull, C. C. Stoumpos, F. Zheng, T. F. Heinz, L. Kronik, M. G. Kanatzidis, J. S. Owen, A. M. Rappe, M. A. Pimenta, L. E. Brus, *Phys. Rev. Lett.* **2017**, *118*, 136001.
[31] B. Dhanabalan, Y.-C. Leng, G. Biffi, M.-L. Lin, P.-H. Tan, I. Infante, L. Manna, M. P. Arciniegas, R. Krahne, *ACS Nano* **2020**, *14*, 4689.
[32] W.-J. Wei, C. Li, L.-S. Li, Y.-Z. Tang, X.-X. Jiang, Z.-S. Lin, *J. Mater. Chem. C* **2019**, *7*, 11964.
[33] H. Abid, A. Trigui, A. Mlayah, E. K. Hlil, Y. Abid, *Results Phys.* **2012**, *2*, 71.
[34] C. Quarti, G. Grancini, E. Mosconi, P. Bruno, J. M. Ball, M. M. Lee, H. J. Snaith, A. Petrozza, F. De Angelis, *J. Phys. Chem. Lett.* **2014**, *5*, 279.
[35] A. M. A. Leguy, A. R. Goñi, J. M. Frost, J. Skelton, F. Brivio, X. Rodríguez-Martínez, O. J. Weber, A. Pallipurath, M. I. Alonso, M. Campoy-Quiles, M. T. Weller, J. Nelson, A. Walsh, P. R. F. Barnes, *Phys. Chem. Chem. Phys.* **2016**, *18*, 27051.
[36] F. Brivio, J. M. Frost, J. M. Skelton, A. J. Jackson, O. J. Weber, M. T. Weller, A. R. Goni, A. M. A. Leguy, P. R. F. Barnes, A. Walsh, *Phys. Rev. B* **2015**, *92*, 144308.
[37] M. A. Peŕez-Osorio, Q. Lin, R. T. Phillips, R. L. Milot, L. M. Herz, M. B. Johnston, F. Giustino, *J. Phys. Chem. C* **2018**, *122*, 21703.
[38] P. DiAntonio, B. E. Vugmeister, J. Toulouse, L. A. Boatner, *Phys. Rev. B* **1993**, *47*, 5629.
[39] B. E. Vugmeister, *Phys. Rev. B* **2006**, *73*, 174117.
[40] A. Hushur, S. Gvasaliya, B. Roessli, S. Lushnikov, S. Kojima, *Phys. Rev. B* **2007**, *76*, 064104.
[41] K. Momma, F. Izumi, *J. Appl. Crystallogr.* **2011**, *44*, 1272.
[42] L. Polimeno, M. De Giorgi, G. Lerario, L. De Marco, L. Dominici, V. Ardizzone, M. Pugliese, C. T. Prontera, V. Maiorano, A. Moliterni, C. Giannini, V. Olieric, G. Gigli, D. Ballarini, D. Solnyshkov, G. Malpuech, D. Sanvitto, *Nat. Nanotechnol.* **2021**, *16*, 1349.
[43] F. Lédée, G. Trippé-Allard, H. Diab, P. Audebert, D. Garrot, J.-S. Lauret, E. Deleporte, *CrystEngComm* **2017**, *19*, 2598.
[44] A. Fieramosca, L. De Marco, M. Passoni, L. Polimeno, A. Rizzo, B. L. Rosa, G. Cruciani, L. Dominici, M. De Giorgi, G. Gigli, *ACS Photonics* **2018**, *5*, 4179.
[45] E. K. Tekelenburg, S. Kahmann, M. E. Kamminga, G. R. Blake, M. A. Loi, *Adv. Opt. Mater.* **2021**, *9*, 2001647.
[46] Q. Tu, I. Spanopoulos, E. S. Vasileiadou, X. Li, M. G. Kanatzidis, G. S. Shekhawat, V. P. Dravid, *ACS Appl. Mater. Interfaces* **2020**, *12*, 20440.
[47] S. Baroni, S. de Gironcoli, A. D. Corso, P. Giannozzi, *Rev. Mod. Phys.* **2001**, *73*, 515.
[48] P. Giannozzi, O. Andreussi, T. Brumme, O. Bunau, M. Buongiorno Nardelli, M. Calandra, R. Car, C. Cavazzoni, D. Ceresoli, M. Cococcioni, N. Colonna, I. Carnimeo, A. Dal Corso, S. de Gironcoli, P. Delugas, R. A. DiStasioJr, A. Ferretti, A. Floris, G. Fratesi, G. Fugallo, R. Gebauer, U. Gerstmann, F. Giustino, T. Gorni, J. Jia, M. Kawamura, H.-Y. Ko, A. Kokalj, E. Küçükbenl, M. Lazzeri, et al., *J. Phys.: Condens. Matter* **2017**, *29*, 465901.
[49] T. Zhu, E. Ertekin, *Energy Environ. Sci.* **2019**, *12*, 216.
[50] A. C. Ferreira, S. Paofai, A. Létoublon, J. Ollivier, S. Raymond, B. Hehlen, B. Rufflé, S. Cordier, C. Katan, J. Even, P. Bourges, *Commun. Phys.* **2020**, *3*, 48.
[51] C. Gehrmann, D. A. Egger, *Nat. Commun.* **2019**, *10*, 3141.
[52] A. M. Sanni, S. N. Lavan, A. S. Rury, *J. Phys. Chem. C* **2020**, *124*, 13942.
[53] E. Molinari, S. Baroni, P. Giannozzi, S. de Gironcoli, in *Light Scattering in Semiconductor Structures and Superlattices* (Eds: D. J. Lockwood, J. F. Young), Springer, Boston **1991**.
[54] M. Nakayama, K. Kubota, S. Chika, H. Kato, N. Sano, *Solid State Commun.* **1986**, *28*, 475.
[55] C. Colvard, T. A. Gant, M. V. Klein, R. Merlin, R. Fischer, H. Morkoc, A. C. Gossard, *Phys. Rev. B* **1985**, *31*, 2080.
[56] K. Pradeesh, K. N. Rao, G. V. Prakasha, *J. Appl. Phys.* **2013**, *113*, 083523.
[57] D. B. Mitzi, *Chem. Mater.* **1996**, *8*, 791.
[58] A. Lemmerera, D. G. Billing, *Dalton Trans.* **2012**, *41*, 1146.

[59] C. Deng, G. Zhou, D. Chen, J. Zhao, Y. Wang, Q. Liu, *J. Phys. Chem. Lett.* **2020**, *11*, 2934.
[60] S. N. Lavan, A. M. Sanni, A. S. Rury, Z.-F. Liu, *J. Phys. Chem. C* **2021**, *125*, 223.
[61] A. K. Sood, J. Menéndez, M. Cardona, K. Ploog, *Phys. Rev. Lett.* **1985**, *54*, 2115.
[62] A. K. Arora, A. K. Ramdas, M. R. Melloch, N. Otsuka, *Phys. Rev. B* **1987**, *36*, 1021.
[63] A. Alexandrou, M. Cardona, K. Ploog, *Phys. Rev. B* **1988**, *38*, 2196.
[64] D. A. Kleinman, R. C. Miller, A. C. Gossard, *Phys. Rev. B* **1987**, *35*, 664.
[65] A. K. Sood, J. Menéndez, M. Cardona, K. Ploog, *Phys. Rev. B* **1985**, *32*, 1412.
[66] P. Giannozzi, S. Baroni, N. Bonini, M. Calandra, R. Car, C. Cavazzoni, D. Ceresoli, G. L. Chiarotti, M. Cococcioni, I. Dabo, A. Dal Corso, S. de Gironcoli, S. Fabris, G. Fratesi, R. Gebauer, U. Gerstmann, C. Gougoussis, A. Kokalj, M. Lazzeri, L. Martin-Samos, N. Marzari, F. Mauri, R. Mazzarello, S. Paolini, A. Pasquarello, L. Paulatto, C. Sbraccia, S. Scandolo, G. Sclauzero, A. P. Seitsonen, et al., *J. Phys.: Condens. Matter* **2009**, *21*, 395502.
[67] J. P. Perdew, K. Burke, M. Ernzerhof, *Phys. Rev. Lett.* **1996**, *77*, 3865.
[68] H. J. Monkhorst, J. D. Pack, *Phys. Rev. B* **1976**, *13*, 5188.
[69] M. Cinquino, A. Fieramosca, R. Mastria, L. Polimeno, A. Moliterni, V. Olieric, N. Matsugaki, R. Panico, M. De, G. Gigli, C. Giannini, A. Rizzo, D. Sanvitto, L. De, *Adv. Mater.* **2021**, *33*, 2102326.